Effect of Compatibilizer on Nanostructure of the Biodegradable Cellulose Acetate/Organoclay Nanocomposites

Hwan-Man Park,[†] Xuemei Liang,[†] Amar K. Mohanty,[‡] Manjusri Misra,[†] and Lawrence T. Drzal*,[†]

Composite Materials and Structures Center, Department of Chemical Engineering and Material Science, 2100 Engineering Building, Michigan State University, East Lansing, Michigan 48824, and The School of Packaging, 130 Packaging Building, Michigan State University, East Lansing, Michigan 48824

Received May 26, 2004; Revised Manuscript Received August 30, 2004

ABSTRACT: Biodegradable nanocomposites were successfully fabricated from cellulose acetate (CA) plasticized with triethyl citrate (TEC), and combined with Cloisite 30B organoclay, using maleic anhydride grafted cellulose acetate butyrate (CAB-*g*-MA) as the compatibilizer. The nanostructure of the nanocomposites was investigated by AFM, TEM, and XRD. AFM analysis clearly showed the presence of exfoliated clay platelets in the nanocomposite. Nanocomposites with 5 wt % compatibilizer contents showed better-exfoliated structure than the counterpart without compatibilizer hybrid. The clay platelet polygonal shape was observable by AFM. The exfoliated platelets were characterized to be ∼1.3 nm in thickness, ∼500 nm in width, and ∼800 nm in length. These results correspond to the XRD and TEM analysis. It was showed that the mechanical properties were improved due to good exfoliation and dispersion of clay in the plasticized CA matrix. The 5 wt % compatibilizer loading is optimum for mechanical improvement.

Introduction

Nanoreinforcement of bio-based polymers with nanoclay, nanotubes, and other nanostructures[1,2] offer potential to increase the utilization of biopolymers due to improvement in their properties such as heat distortion temperature, dimensional stability, barrier properties, flame retardancy, and physico/thermomechanical properties. Renewable resource-based biodegradable polymers, such as cellulosic plastic (plastic made from wood), polylactic acid (PLA; corn-derived plastic), and poly(hydroxyalkanoate) (PHA; bacterial polyesters), are biopolymers, which have potential to be used as alternatives to petroleum-based polymers such as polypropylene after effective reinforcement with nanoclays.[3−5] Cellulose from trees is attracting interest as a feedstock for making polymers (cellulosic plastic−cellulose esters) that can substitute for petroleum-based polymers in the commercial market.[6] Cellulosic derived plastics such as cellulose acetate (CA), cellulose acetate propionate (CAP), and cellulose acetate butyrate (CAB) are thermoplastic materials produced through esterification of cellulose. CA is of particular interest because it is a biodegradable polymer and has excellent optical clarity and high toughness. However, the main drawback of cellulose acetate plastic is that its typical melting range is near its decomposition temperature. Plasticizer is added to overcome this problem. The phthalate plasticizer, normally used in commercial cellulose ester plastic, is now under scrutiny for its potential health and environmental impact.

One of the goals of this research is to find a viable replacement for phthalate plasticizer with eco-friendly plasticizers such as citrate,[7] and/or blends of citrate, and derivatized vegetable oil.[8] The other objective is to develop a suitable compatibilizer for producing exfoliated clay in the organic/inorganic nanocomposites.

Maleic anhydride grafted cellulose acetate butyrate (CAB-*g*-MA) was synthesized as the compatibilizer in order to obtain interaction between CA and the organoclay to produce exfoliated and/or intercalated clays in this matrix. Maleic anhydride (MA) is a common monomer for grafting reactions because the monomer itself does not homopolymerize under the reaction conditions used in grafting reactions.[9] In the same way that maleated propylene (MAPP) is an effective compatibilizer for organoclay−polypropylene (PP) nanocomposites, the maleated CAB is expected to be more effective because CA is polar while PP is nonpolar.

In this investigation of cellulose acetate plastic-clay-based nanocomposites, triethyl citrate has been selected as the plasticizer and melt processing via extrusion−injection molding has been selected as the processing method for fabricating the nanocomposites. Organically modified montmorillonite clays are compounded into the plasticized CA matrix under conditions of high shear melt extrusion in order to disperse the exfoliated and/or intercalated clays into the polymer matrix (see Scheme 1a).

Nanostructural morphological information is important for a complete understanding of the relationship between the solid-state structure and its physical properties. However, studies of lamellar structure have been limited by the availability of high-resolution experimental probes, which can directly image at the nanometer length scale. Because atomic force microscopy (AFM) has comparable spatial resolution to transmission electron microscopy (TEM) and no special sample preparation is required, this technique, particularly tapping mode AFM, has received considerable attention in the study of the lamellar morphology of semicrystalline polymers recently.[10,11]

A number of studies have shown that useful information can be obtained from tapping mode images of soft

[†] Department of Chemical Engineering and Material Science.
[‡] The School of Packaging.
* To whom all correspondence should be addressed: e-mail drzal@egr.msu.edu; Tel (517) 353-5466; Fax (517) 432-1634.

10.1021/ma048958s CCC: $27.50
Published on Web 11/04/2004

Scheme 1. (a) Schematic Representation: Mechanism of Compatibilized CA/TEC/Organoclay Hybrid Nanocomposites; (b) Proposed Mechanism of the Interaction between the Modifier of Organoclay Cloisite 30B and the CAB-*g*-MA

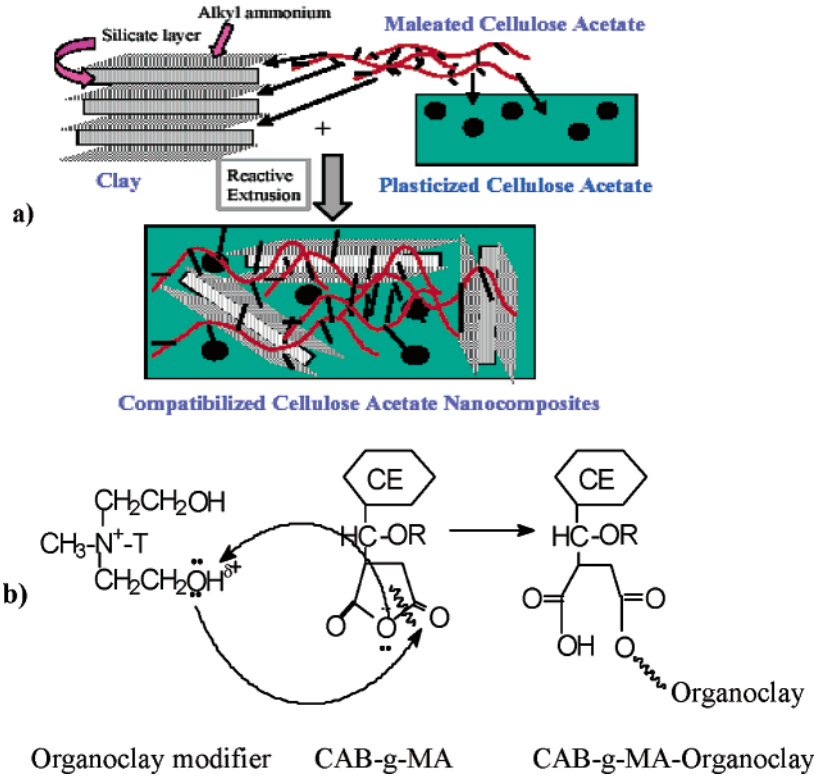

samples, especially with samples showing phase contrast at small scale such as blends of hard and soft materials including clay.[12−15] But there have been no reports on the preparation and nanostructural characterization of CA/organoclay/with or without compatibilizer.

In this study, novel procedure to fabricate nanocomposites using CAB-*g*-MA as compatibilizer is reported which results in superior exfoliated clay hybrids.

Experimental Section

Materials. Cellulose acetate, CA (CA-398-30, acetyl 39.7 wt %, hydroxyl 3.5 wt %, DS = 2.45), and cellulose acetate butyrate, CAB (CAB-381-20, butyryl 37 wt %, acetyl 13.5 wt %, hydroxyl 1.8 wt %), without additives in powder form and triethyl citrate (TEC, Citroflex 2) were supplied by Eastman Chemical Co. (Kingsport, TN) and Morflex, Inc. (Greensboro, NC), respectively. The biodegradability of CA depends on the degree of substitution (DS). Organically modified montmorillonite (organoclay) Cloisite 30B was obtained from Southern Clay Co. (Gonzales, TX). The ammonium cations present in Cloisite 30B are methyl tallow bis(2-hydroxyethyl) quaternary ammonium. Maleic anhydride (99%, MA), liquid initiator (2,5-dimethyl-2,5-di(*tert*-butylperoxy)hexane (Luperox 101)), acetone, and 0.1011 N methanolic KOH were obtained from the Aldrich Chemical Co.

Synthesis and Characterization of Compatibilizer (CAB-*g*-MA). **CAB**-*g*-MA was synthesized by radical graft polymerization of the MA monomer onto the CAB backbone polymer and characterized (see Supporting Information).[16] The solvent-free synthesis of MA-*g*-CAB was conducted in a DSM Micro 15 cm^3 extruder−compounder (DSM Research, The Netherlands). The mixture of CAB, MA (both in powder form), and Luperox 101 initiator was processed at temperatures between 195 and 205 °C and a screw speed of 100 rpm and with a cycle time of 3 min. Thin strands of extrudate were collected and pelletized into granules which were subsequently vacuum-dried at 80−90 °C for 24 h to remove unreacted maleic anhydride. A portion of the vacuum-dried CAB-*g*-MA was used for quantitative CAB-*g*-MA characterization by acid−base titration to determine acid number (AN) and percentage MA grafting (wt % MA). The method adopted by Carlson et al.[17] was modified in order to characterize CAB-*g*-MA by acid−base titration. The calculated acid number and grafting percentage (MA wt %) were 18.6 and 0.86 wt %, respectively (see detailed method).[16]

In Figure 1, the IR spectra of ∼100 nm melt cast thin film samples differentiates between carbonyl groups of neat CAB and those of MA. Carbonyl groups which belong to MA were assigned to the region around 1786−1782 cm^{-1}, whereas the peak at 1770 and 1766 cm^{-1} was assigned to carbonyl groups of neat CAB while the peak at 1731 cm^{-1}(not shown here) was assigned to the carbonyl groups of neat CA. Silverstein et al. report that the IR spectra of the grafted MA-ester show bands

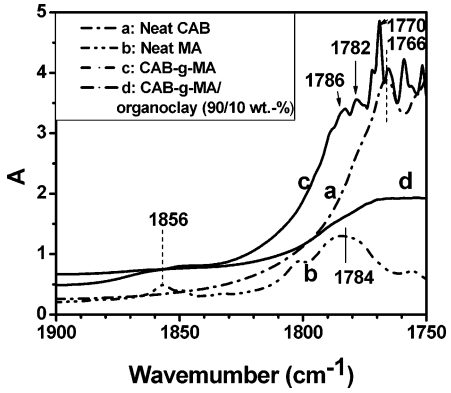

Figure 1. FTIR analysis of CAB, MA, compatibilizer CAB-*g*-MA, and CA/CAB-*g*-MA/organoclay nanocomposites: (a) neat CAB, (b) neat maleic anhydride, (c) CAB-*g*-MA (MA 0.8 wt % grafted), (d) CAB-*g*-MA/organoclay nanocomposites (90/10 wt %). (note: 1766, 1770 cm^{-1} is C=O of CAB; 1786, 1782 cm^{-1} is C=O of MA).

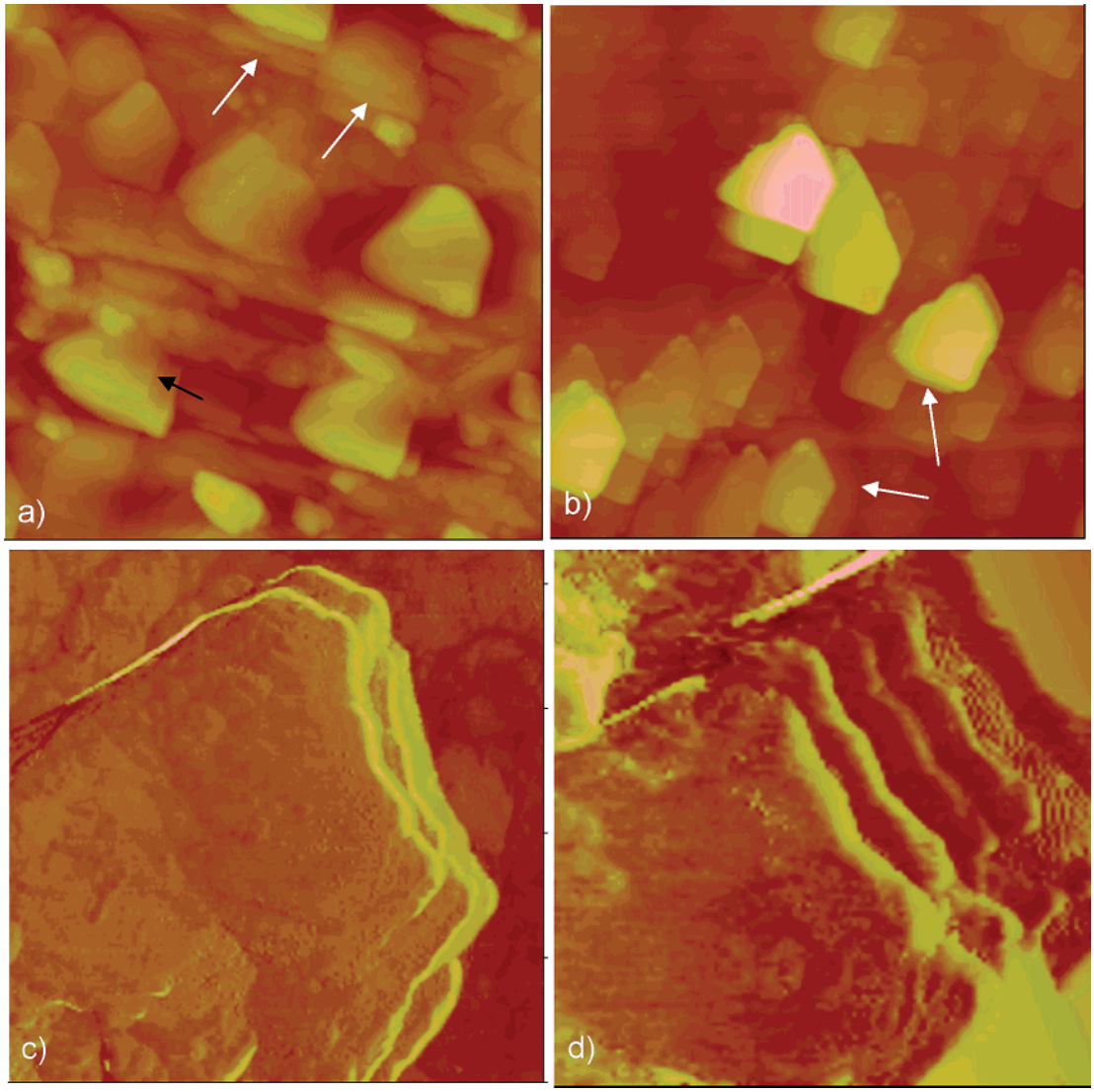

Figure 2. AFM height and phase images of plasticized CA/compatibilizer/organoclay system: (a) topographical height view of nanocomposite without compatibilizer, scan size 5 μm; (b) topographical height view of nanocomposite with compatibilizer 5 wt %, scan size 5 μm; (c) phase image of intercalate clay without compatibilizer, scan size 0.85 μm; (d) phase image of intercalate clay with compatibilizer 5 wt %, scan size 0.5 μm.

at 1788 cm^{-1} corresponding to the symmetric C=O stretch of a saturated cyclic five membered anhydride.[18]

Melt Compounding. CA, CAB-*g*-MA, and organoclay were dried in a vacuum oven at 80 °C for 24 h before use. The CA powder and TEC plasticizer (CA/TEC = 75/25 wt %) were mixed mechanically with a high-speed mixer for 5 min, and this mixture was stored in a zip-lock bag for 75 min. The preplasticized mixtures were then mixed with 5 wt % organoclays and compatibilizer CAB-*g*-MA (0−7.5 wt %) followed by mixing with the high-speed mixer. The mixtures of various formulations (preplasticized CA + organoclay + compatibilizer) were melt compounded and plasticized simultaneously at 200−210 °C for 6 min at 100 rpm with the microcompounding molding equipment. This powder−powder melt compounding method is ideal to produce high dispersion of the clay particles.

Characterization of Nanocomposites. The samples made by injection molding were subjected to different characterization methods. AFM characterization was conducted using a Nanoscope IV atomic force microscope from Digital Instruments (Santa Barbara, CA) equipped with an E scanner. Samples were mounted onto a stainless steel disk using a sticky tab (Latham, NY). The microscope was allowed to thermally equilibrate for 30 min before imaging. Scanning rates less than 1 Hz were used. Room temperature was maintained at 22 ± 1 °C. Images were recorded in tapping mode using etched silicon probes (Digital Instruments). The parameters, especially the set point and the gains, were adjusted to obtain the best image resolution. For every sample, images were collected at different locations to obtain reproducible and reliable images. Most images are presented without further treatment unless specified. The sample surfaces were prepared by cross-plane sectioning with a diamond knife at room temperature. The sample surface was polished with 4000# grit paper until a smooth surface was obtained.

XRD studies of the samples were carried out using a Rigaku 200B X-ray diffractometer (45 kV, 100 mA) equipped with Cu Kα radiation (λ = 0.1541 nm). A transmission electron microscope (TEM) (JEOL 100CX and 2010F) was used to analyze the morphology of nanocomposites at an acceleration voltage of 100 kV for 100CX and 200 kV for 2010F. Microtomed ultrathin film specimens with thickness of 70 nm for cross section or 20 nm for plane section were used for the TEM characterization. Fourier transform infrared spectrum (FTIR, Perkin-Elmer system 2000 spectrometer) was measured on a melt cast thin film. Tensile properties and flexural properties of injection mold specimens were measured with a United Testing System SFM-20 according to ASTM D638 and ASTM D790, respectively. System control and data analysis were performed using Datum software.

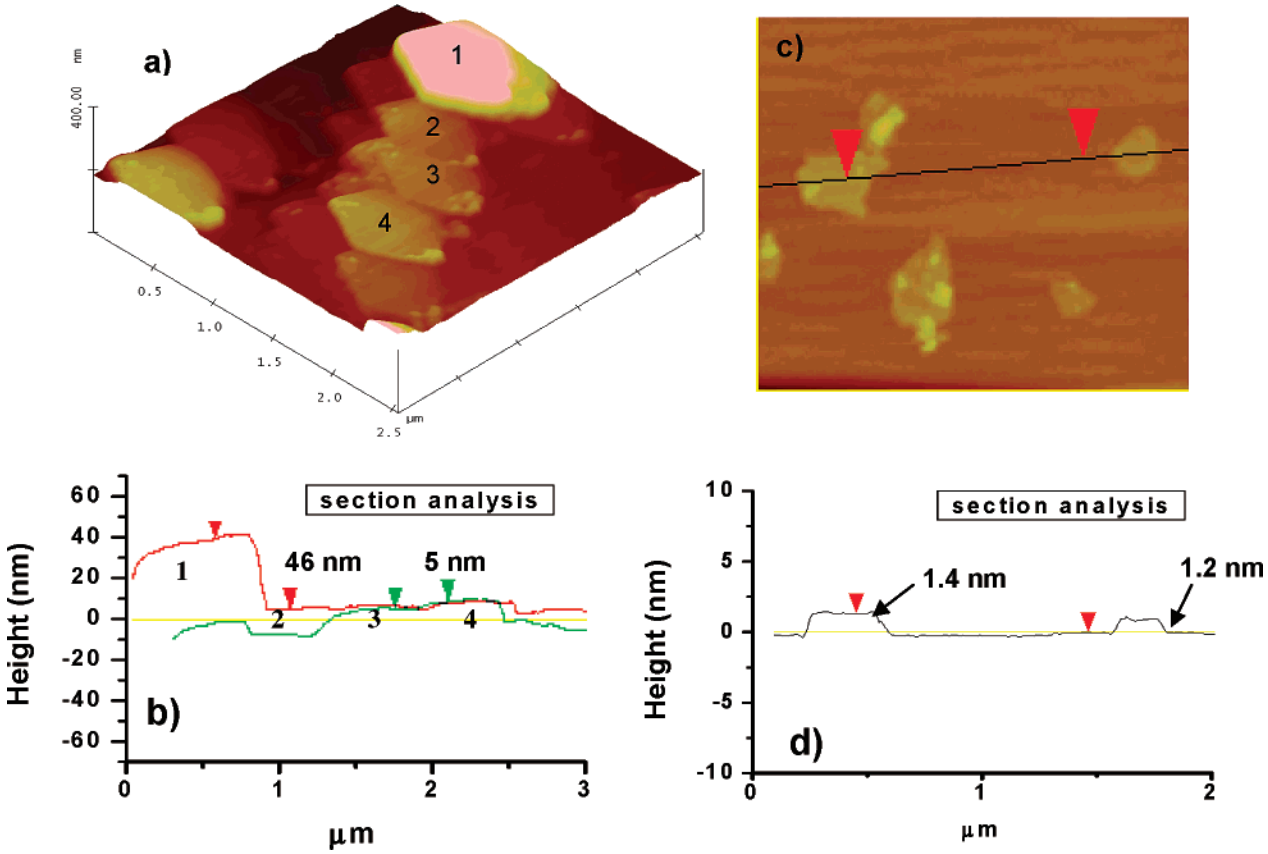

Figure 3. 3D AFM height image and section analysis: (a) and (b) the intercalated and exfoliated clay platelets in CA/organoclay hybrid with 5 wt % compatibilizer, scan size 2.5 um; (c) and (d) completely exfoliated clay platelets in the mica surface, scan size 2.0 um.

Results and Discussion

Nanostructure of Hybrids. To obtain the better exfoliated nanocomposites, the synthesized compatibilizer was added to the preplasticized CA/Cloisite 30B composition at 0, 5, and 7.5 wt % content. The 5 wt % compatibilizer CAB-*g*-MA (grafting percentage (MA wt %) was 0.86 wt %) hybrid nanocomposite show the best morphology and mechanical properties. Therefore, nanocomposites with 5 wt % compatibilizer or without compatibilizer were used to investigate the nanostructure.

Figure 2 shows AFM height images of the nanocomposites without compatibilizer (Figure 2a) and with 5 wt % compatibilizer (Figure 2b). An advantage of AFM imaging is the relatively high phase contrast[19] between the soft matrix and the hard silicate particles of the nanocomposites. The images show that the plasticized CA/organoclay/compatibilizer hybrid has better exfoliation nanocomposites than the counterparts without compatibilizer. The intercalated structure of clay is dominant in Figure 2a as labeled by the arrows. Partially exfoliated clay can be seen clearly in Figure 2b (showed by arrows), coexisting with the intercalated clay particles. The results are consistent with TEM images (Figure 6). It can be seen from the images that the clay reinforcement in the absence of compatibilizer tends to aggregate, which can be overcome by addition of the compatibilizer (Figure 6c, TEM image; Figure 2b, AFM image). The width of the clay nanoplatelets is around 500 nm, and the length is around 800 nm. It is obvious that the pentagon-shaped clay platelets have been oriented along one direction. This is due to the external force applied to the nanocomposite samples in the injection molding process. This ordered exfoliated morphology influenced the mechanical and barrier properties of nanocomposites.

Parts c and d of Figure 2 show the cross-section AFM phase images of the intercalated CA/organoclay without and with 5 wt % compatibilizer, respectively. Well-defined intercalated clay platelet structure was observed. However, large separations (Figure 2d) between intercalated clay platelets were observed for the nanocomposite with 5.0 wt % compatibilizer compared to that without compatibilizer (Figure 2c).

AFM was also employed to determine the gallery spacing between intercalated and exfoliated clay platelets. Parts a and b of Figure 3 illustrate the intercalated and exfoliated clay platelet in CA/clay/5 wt % compatibilizer systems. Several clay platelets are clearly showed in Figure 3a, signified by numbers. The section analysis of gallery space between platelet 1 and 2 is around 46 nm, and the space between 3 and 4 is around 5 nm (Figure 3b). Thus, the compatibilizer aided the exfoliation which was consistent with XRD analysis (Figure 5c) and TEM image (Figure 6c).

Individual platelet thickness could not be detected from this hybrid image; therefore, completely individual exfoliated platelets were made from TEC plasticizer/organoclay (Closite 30B) to measure the thickness of the individual organoclay platelet. First, 5 mg of organoclay was exfoliated with 10 g of TEC for 24 h and then ultrasonicated for 10 h in a solution made by a 50× dilution with acetone. This suspension was stored at room temperature without mixing for about 2 weeks. Finally, the upper solution of this suspension was spin-coated on a mica surface. Parts c and d of Figure 3 show

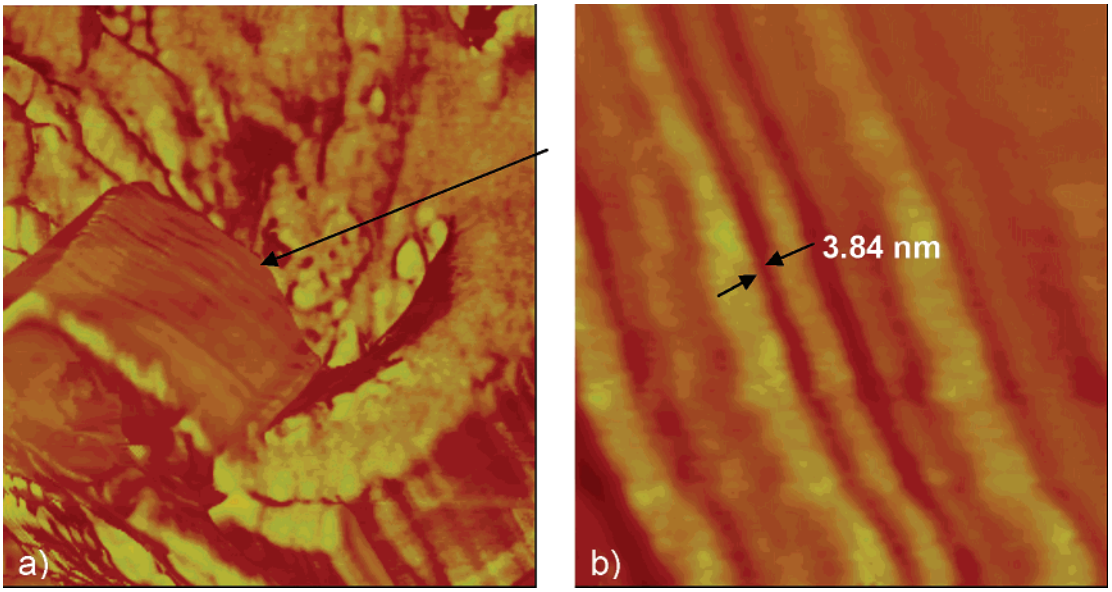

Figure 4. Phase images of CA/organoclay without compatibilizer system. (a) Scan size is 1.5 μm; the arrow labeled the magnified image of the clay aggregate. (b) Magnified image of the layer structure of clay aggregate. Scan size 150 nm.

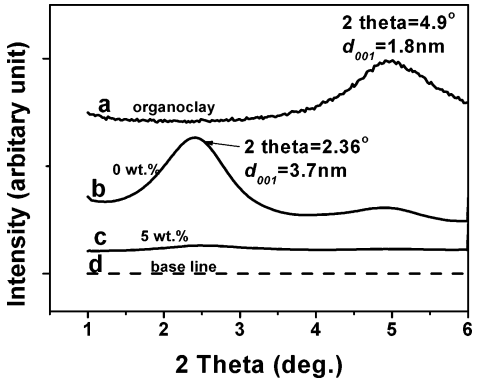

Figure 5. XRD patterns of the plasticized CA/compatibilizer/Cloisite 30B hybrids with different compatibilizer CAB-*g*-MA: (a) neat organoclay (Cloisite 30B), (b) compatibilizer 0 wt %, and (c) compatibilizer 5 wt %.

the image and sectional analysis of completely exfoliated individual platelets after spin-coating, respectively. It was found that the thickness of organoclay platelets is 1.2−1.4 nm (average 1.3 nm), which is similar to our XRD analysis (Figure 5a). The thickness of completely exfoliated natural clay (Cloisite Na^+, not organo-modified clay) platelets is reported as 1 nm.[15] The thickness of organoclay (Cloisite 30B) is slightly thicker than Cloisite Na^+; the reason may be due to the organic modified chain length of the organoclay added to the natural clay thickness. From XRD analysis, the gallery space between the two clay platelets is 1.8 and 3.7 nm for pure organoclay and CA/clay, respectively (see Figure 5, a and b). When 5 wt % compatibilizer was added, a very small peak around 2.36° was observed, which explains the coexistence of intercalated and exfoliated clay platelets in the CA/clay/5 wt % compatibilizer system.

A highly ordered intercalated clay platelet structure was observed for nanocomposites without compatibilizer, as shown in Figure 4. Dark lines are polymer intercalated with a one-layer thickness (about 3.84 nm), and yellow features indicate multilayered silica clay platelets. The stiffer crystalline clay component appears as a bright color and the soft polymer as a dark color in the AFM tapping phase image. This agrees with XRD results (Figure 4b, d_{001} spacing of intercalated clay is 3.7 nm, $2\theta = 2.36°$). This result is also consistent with the TEM image of the intercalated platelet without compatibilizer, which showed a total 30 nm thickness for 5−6 layers and an individual thickness of intercalated clay of about 5−6 nm (Figure 6b). Dietsche et al. reported that an AFM image of a poly(methyl methacrylate) copolymer/bentonite (via ion exchange with *N,N,N,N*-dioctadecyldimethylammonium chloride) showed laminated and intercalated layered silicates nanoparticles of 400 nm in length and 5−10 nm in thickness.[20] Our thickness 5−6 nm of hybrids is similar to that reported by Dietsche.

Figure 5 shows the XRD patterns of pure Cloisite 30B clay and plasticized CA/Cloisite 30B nanocomposites with different amounts of CAB-*g*-MA. The XRD peak shifted from 5.0° (d_{001} spacing = 1.7 nm) for pure Cloisite 30B to 2.36° (d_{001} spacing = 3.7 nm) for plasticized CA/organoclay (95/5 wt %) nanocomposite without compatibilizer (Figure 5b). This indicates significant intercalation and slight exfoliation in the hybrid structure. For plasticized CA/Cloisite 30B/compatibilizer nanocomposites with 5 wt % of compatibilizer, a small peak observed at 2.36° (Figure 4c) presumably corresponds to the poor regularity of the intercalated organoclay structures remaining in the CA/TEC matrix. Using the Bragg equation (i.e., $1 \times \lambda = 2d_{001} \sin \theta$, here $\lambda = 1.541$ nm, X-ray source; θ = XRD diffraction angle), the theoretical diffraction angle for this large intercalated part (46 nm from AFM image, refers to which Figure) 2θ of XRD is calculated to be 0.05°. Therefore, these large intercalated clay platelets of hybrids from the AFM and TEM images cannot be detected by wide-angle XRD ($2\theta > 1.0°$).

Figure 6 explains the morphology of the nanocomposites. The TEM images show that the plasticized CA/organoclay/compatibilizer hybrid (Figure 6c) undergoes better exfoliation and dispersion than the counterparts without compatibilizer (Figure 6a,b). From Figure 6a, it can be seen that some of the intercalation and aggregation of clay remain in the matrix. It can also be observed from Figure 6b that small intercalated organoclay platelets in the CA matrix show a total 30 nm

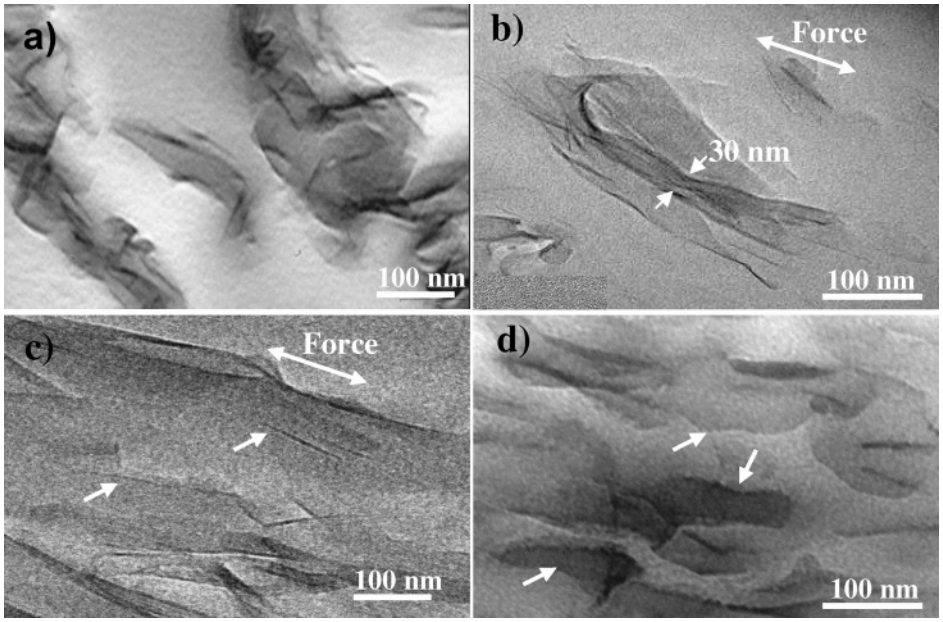

Figure 6. TEM of the plasticized CA/compatibilizer/organoclay hybrids with or without compatibilizer: (a) without compatibilizer, cross section, 100 kV; (b) intercalated part of without compatibilizer, cross section, 200 kV; (c) exfoliated part of with compatibilizer, cross section, 200 kV; (d) exfoliated part of with compatibilizer, plane section, 100 kV.

Table 1. Tensile and Flexural Properties of Plasticized CA/Cloisite 30B/Compatibilizer MA-*g*-CAB Hybrids

plasticized CA/organoclay/ compatibilizer (wt %)	tensile strength (MPa)	tensile modulus (GPa)	tensile elongation (%)	flexural strength (MPa)	flexural modulus (GPa)
100/0/0	70.0 ± 5.1	2.20 ± 0.1	8.8 ± 1.2	65.4 ± 2.0	2.37 ± 0.2
95/5/0	81.8 ± 5.9	3.6 ± 0.6	10.0 ± 0.2	74.7 ± 0.9	2.68 ± 0.5
90/5/5	84.7 ± 0.9	3.7 ± 0.6	9.5 ± 1.2	81.7 ± 0.9	3.09 ± 0.6
87.5/5/7.5	84.2 ± 1.9	3.7 ± 0.4	8.6 ± 0.9	77.4 ± 1.2	2.97 ± 0.4

distance of about 5−6-layer clay; the individual intercalated thickness is approximately 5−6 nm. Figure 6d is a plane-sectioned TEM displaying the morphology with compatibilizer hybrid nanocomposites. These polygonal platelets in the plane-view clay are dispersed in the matrix (see arrows), supporting the AFM data (Figures 2b and 3a,c).

From AFM, XRD, and TEM results, the concentration of compatibilizer (CAB-*g*-MA) is important to produce an exfoliated CA/organoclay hybrid nanocomposites. The maleated CAB will not only react with the organoclay but also will react with the free OH groups of the CA structure, thus improving the overall compatibilization of the entire system. CA matrix has polar functional hydroxyl groups that contribute to the interaction between the matrix and organoclay in the presence of the compatibilizer at higher shear conditions under high compounding temperature in the extruder. The FTIR curve (Figure 1d) shows the disappearance of the CO group of the MA 1786−1782 cm^{-1} peak in the CAB-*g*-MA/organoclay (90/10 wt %) may be due to the ring-opening reaction of the CO group in MA-*g*-CAB with the free OH of organoclay (this OH comes from organo modifier, i.e., methyl tallow bis(2-hydroxyethyl) quaternary ammonium of Cloisite 30B) to produce a new aliphatic ester structure (this peak is shown at the broad complex peak 1770−1725 cm^{-1}). It is assumed that the hydroxyl (−OH) groups of CA are sterically rigid and minimally accessible but the anhydride of the compatibilizer would react with the organic modifier of Cloisite 30B organoclay as shown in Scheme 1b. However, measuring the extent of this reaction is difficult.

Mechanical and Thermal Properties of Nanocomposites. Table 1 shows the tensile and flexural properties of the plasticized CA/Cloisite 30B/MA-*g*-CAB hybrids with variation compatibilizer MA-*g*-CAB contents. The 5 wt % compatibilizer loading is optimum for mechanical improvement. These properties of higher compatibilizer loading (7.5 wt %) nanocomposites were decreased. It may be due to poor exfoliation and dispersion of nanocomposites because higher loading of compatibilizer brings higher melt compound viscosity. The strength and modulus (flexural and tensile) of the hybrid sharply increased with compatibilizer contents. On the other hand, the tensile elongation at break of the hybrids decreased with compatibilizer contents. This indicates that compatibilizer is effective in increasing the adhesion between organoclay and CA molecular chains. The tensile strength and modulus of hybrids with 5 wt % compatibilizer increased by 20% and 68%, respectively, compared to hybrids with no compatibilizer. Also, the flexural strength and modulus were increased about 20% and 25%, respectively. In summary, good mechanical properties were obtained because of better exfoliation and good dispersion of clay in the plasticized CA matrix.

Conclusions

Nanocomposites produced from cellulose acetate powder, triethyl citrate plasticizer, compatibilizer, and organically modified clay have been investigated. AFM characterization results corresponded to the XRD and TEM analysis. 5 wt % compatibilizer loading is optimum for mechanical improvement. Nanocomposites with 5 wt % compatibilizer contents showed better-exfoliated structure than the counterpart without compatibilizer hybrid. The mechanical properties were improved due to good

exfoliation and dispersion of clay in the plasticized CA matrix.

The results presented here for cellulose plastic/exfoliated clay nanocomposites clearly support the potential of these new materials to replace polypropylene−clay nanocomposites for future "green" material applications.

Acknowledgment. Authors are thankful (NSF-NER 2002 Award # 0210681 and NSF 2002 award # DMR-0216865, under "Instrumentation for Materials Research (IMR) Program") for financial support. The collaboration with Ford Motor Co. and Eastman Chemical Co. is gratefully acknowledged. The authors are also thankful to Eastman Chemical Co., Kingsport, TN, for the cellulose ester samples as well as to Mr. Arief Wibowo, CMSC, MSU, for preparing the maleated CAB for this research.

Supporting Information Available: Proposed CAB-*g*-MA mechanism of MA grafted onto CAB. This material is available free of charge via the Internet at http://pubs.acs.org.

References and Notes

(1) Czerw, R.; Guo, Z. X.; Ajayan, P. M.; Sun, Y. P.; Carroll, D. L. *Nano Lett.* **2001**, *1*, 423.
(2) Ray, S. S.; Maiti, P.; Okamoto, M.; Yamada, K.; Ueda, K. *Macromolecules* **2002**, *35*, 3104.
(3) Mohanty, A. K.; Drzal, L. T.; Misra, M. *Polym. Mater. Sci. Eng.* **2003**, *88*, 60.
(4) Park, H. M.; Li, X.; Jin, C. J.; Cho, W. J.; Ha, C. S. *Macromol. Mater. Eng.* **2002**, *287*, 553.
(5) Ray, S. S.; Okamoto, M. *Macromol. Rapid Commun.* **2003**, *24*, 815.
(6) Wilkinson, S. L. *Chem. Eng. News* **2001**, January 22, 61.
(7) Mohanty, A. K.; Wibowo, A.; Misra, M.; Drzal, L. T. *Polym. Eng. Sci.* **2003**, *43*, 1151.
(8) Bruins, P. F. In *Plastic Technology*; Reinhold Publishing Co.: New York, 1965; Vol. 1, pp 1−7, 193−199.
(9) Resell, K. E. *J. Polym. Sci., Part A: Polym. Chem.* **1995**, *33*, 555.
(10) Li, H. Q. http://www.chembio.uoguelph.ca/educmat/chm729/afm/moredet.htm.
(11) Kanchanasopa, M.; Manias, E.; Runt, J. *Biomacromolecules* **2003**, *4*, 1203.
(12) Kopp-Marsadon, S.; Leclere, P.; Dubourg, F.; Lazzaroni, R.; Aime, J. P. *Langmuir* **2000**, *16*, 8432.
(13) Knoll, A.; Magerle, R.; Krausch, G. *Macromolecules* **2001**, *34*, 4159.
(14) Kim, D. W.; Blumstein, A.; Tripathy, S. K. *Chem. Mater.* **2001**, *13*, 1916.
(15) Piner, R. D.; Xu, T. T.; Fisher, F. T.; Qiao, Y.; Ruoff, S. *Langmuir* **2003**, *19*, 7995.
(16) Wibowo, A.; Mohanty, A. K.; Misra, M.; Drzal, L. T. *Polym. Prepr.*, Spring **2004**, *45* (1), 1058; 227th ACS Spring National Meeting, Anaheim, CA, 2004.
(17) Carlson, D.; Nie, L.; Narayan, R.; Dubois, P. *J. Appl. Polym. Sci.* **1999**, *72*, 477.
(18) Silverstein, R. M. *Spectrometric Identificatin of Organic Compounds*; Wiley: New York, 1981.
(19) Bar, G.; Thomann, Y.; Brandsch, R.; Cantow, H.-J.; Whangbo, M. H. *Langmuir* **1997**, *13*, 3807.
(20) Dietsche, F.; Thomann, Y.; Thomann, R.; Lhauot, R. M. *J. Appl. Polym. Sci.* **2000**, *75*, 396.

MA048958S